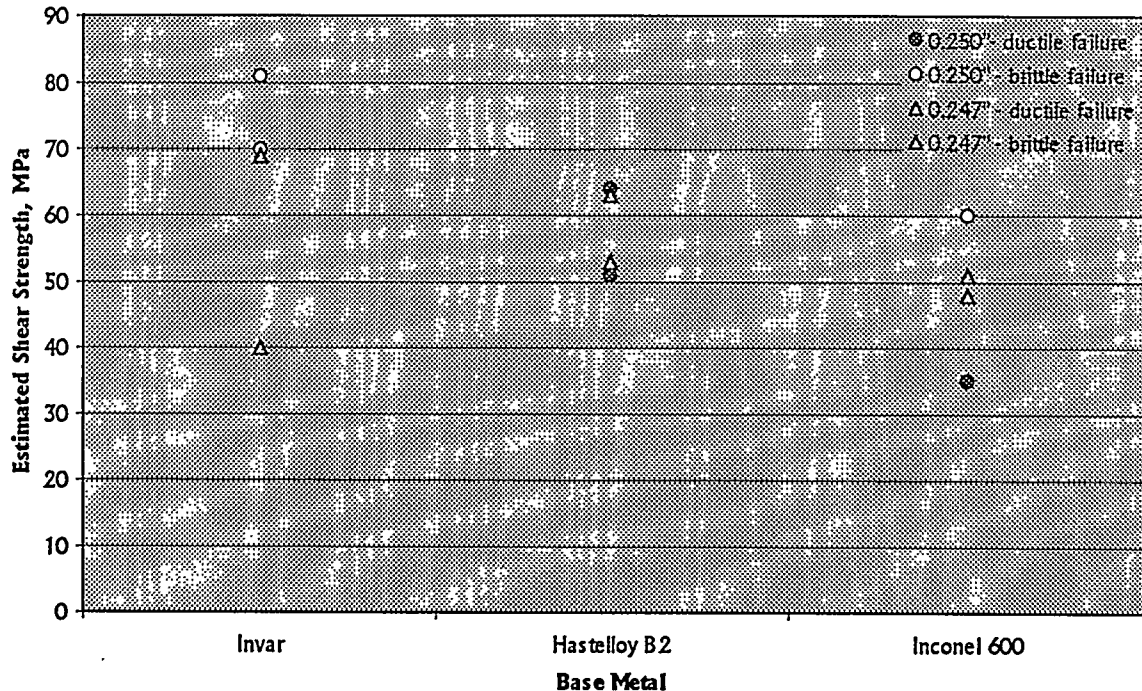


Some samples for condition 1 have already been made and tested. The following graph shows the experimental estimated shear strengths of the joints:

**Table 2: Estimated Shear Strengths of Metal-Ceramic Joints**



These few data points show some general trends about the character of metal-ceramic joints. As the CTE mismatch between the metal and ceramic increase, the strength of the resultant joint decreases. Also, for this geometry, a negative CTE mismatch (ceramic expands more than metal, i.e. the Invar/Alumina joint) does not seem to be as detrimental as a positive mismatch. The filler metal thickness only seems to affect the strength of the Invar/Alumina joint.

Two distinct fracture modes were observed in these samples: brittle failure in the ceramic and ductile failure in the braze. We hope to correlate the CTE mismatch and filler metal thickness of the joint to the failure mode once more data is available.

### Finite Element Modeling

Finite element models for metal-ceramic joints are being made using the ABAQUS software package. Residual stresses develop in these joints during cooling. The system can be considered to be stress-free at the solidus temperature of the braze alloy (780°C for Ticusil™). However, as the joint cools, one member often contracts more than the other, which can result in complicated residual stresses when the joint is at room temperature. The metal usually contracts more than the ceramic, since the CTE of the metal is usually larger than that of the ceramic.

The newest model has the same geometry as the samples used for mechanical testing. It models the stresses developed upon cooling from 780°C to 20°C, and temperature-dependant materials

properties are taken into consideration. It is assumed that both the alumina and base metal are perfectly elastic, and the Ticusil™ layer is perfectly plastic. The finite elements are 8-node axisymmetric elements with reduced integration, and the nodes lying on the Z-axis are constrained in the radial direction.

The magnitude of CTE mismatch between the ceramic and metal greatly influences the residual stresses that are present after cooling. The following figures depict the axial stresses that are present after brazing. The contour map on the right is of a Hastelloy B2 / Ticusil™ / alumina joint (the metal is on the upper right, ceramic on lower left). The metal along the interface is stressed in tension, because it wants to contract but is constrained by the ceramic. The Ticusil™ bonding the components has plastically deformed to accommodate the different contractions of the metal and ceramic.

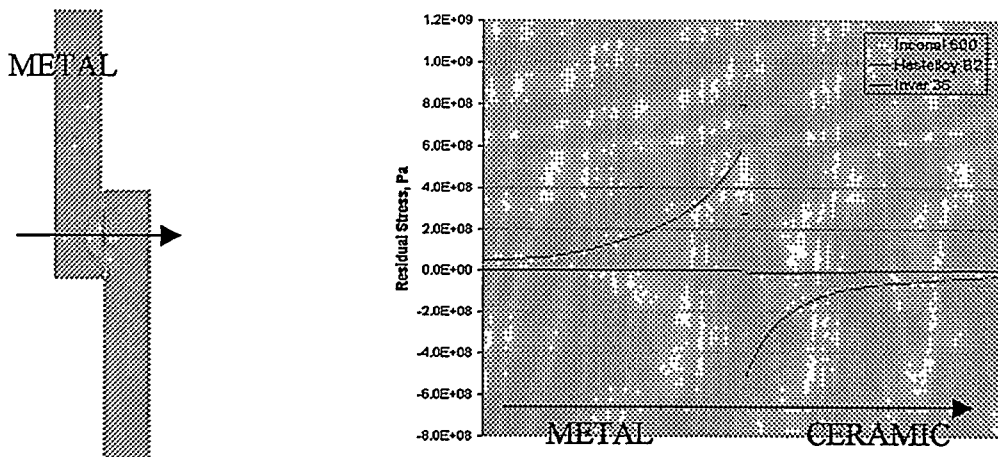


Figure 6: (L) Contour map of residual axial stresses in a Hastelloy B2 / Ticusil™ / Alumina joint.

(R) Residual axial stresses along the midpoint of the braze.

The graph to the left of the contour map compares the axial stresses present across the midsection of a brazed joint for the three different base metals. It is clear that the joints in which the CTE of the metal is much greater than that of the ceramic (Hastelloy B2 and Inconel 600) have much larger residual stresses present than joints where the CTE of the metal is smaller than that of the ceramic (Invar 36).

It follows that joints that have small residual stresses will be stronger than those that have large residual stresses, and this prediction agrees with early experimental results.

**Future Work:**

Using the results obtained from the experimental work, new joining techniques will be designed and tested. Different brazing alloys will be put to test. A complete analysis of the interfaces created will be performed. The mechanical tests will continue, and the strength and thermal fatigue properties of joints will be characterized. From the experiments and numerical analysis on concentric ceramic/metal joints, design rules will be developed.

### **Conclusions:**

Preliminary La-Sr-Fe-O/Haynes 230 joints have been made using amorphous nickel-based filler metals. The fact that these conventional alloys are capable of wetting the ceramic is a positive and a somewhat surprising outcome, although further analysis is required to understand better the phenomena taking place at the ceramic/metal interface.

It has been found that there is a large chemical interaction between the ceramic surface and the braze. This reactivity appears to be affected by the actual oxygen partial pressure under which the joining process takes place, although this has yet to be confirmed. There is also evidence that the extent of the interfacial reactions between the brazing alloy and the ceramic might influence the integrity of the ceramic/metal joint created. An experimental setup for measuring the mechanical properties of concentric ceramic/metal joints has been built and operated. Finite element models of concentric ceramic/metal joints have been made. It is expected that the same experimental program can be performed on the ceramic membrane once the first perovskite tubes are fabricated and sent to us.

### **TASK 3: Determine material mechanical properties under conditions of high temperature and reactive atmosphere**

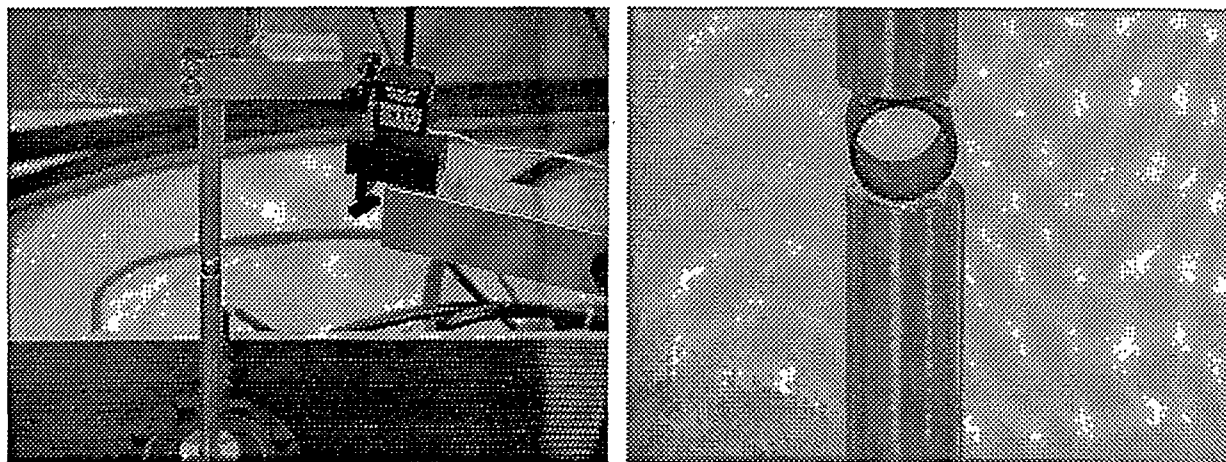
**Prof. Sukumar Bandopadhyay & Dr. Nagendra Nagabhushana  
University of Alaska Fairbanks**

#### **ABSTRACT**

In the fourth quarter, first experiments on the mechanical strength of La-Sr-Fe-O ceramic tubes are reported. Tubes of  $\text{Cr}_2\text{O}_3$  doped  $\text{LaSrFeO}_3$  (20576-25 Px and 20576-25t) were supplied by BP for strength characterization. The tubes were tested at room temperature in C-Ring geometry according to ASTM C1323. The results indicate that tubes 20576-25t exhibited higher fracture as compared to 20576-25Px. A distinctive change in fracture morphology was also observed.

#### **Experimental Set up:**

The Perovskite oxide tubes 20576-25 Px and 20576-25t were cut in to C-Ring specimens. The cut surfaces were polished and the edges beveled. The room temperature experimental set up are as show in figure 1 a and b. The C-ring specimens are placed between two hardened platens and a thin strip of compliant paper inserted to reduce friction and to align the specimens. The tubes were loaded monotonically to fracture and the maximum load recorded to calculate the fracture Stress. The fracture surfaces were examined to characterize the fracture characteristics.



(a)

(b)

Fig.1 Experimental set up for characterizing fracture strength in C-ring specimen geometry.

## OBSERVATIONS

The tubes 20576 were cut into C-rings for mechanical strength characterization. C-ring specimen loaded in diametral compression leads to a maximum tensile stress at the outer surface. The strength distribution and flaw population of the tubes can thus be evaluated on the outer surface of the tube.

The tubes provided were not uniform through out the length and C-ring specimens showed a variation in the wall thickness. As shown in the figure below, C-rings from 20576-25 Px were uniform in the outer diameter, but showed a large variation in the wall thickness. On the other hand, 20576-25t showed fewer scatters in the wall thickness but was not uniform in the outer diameter. These variations were expected to be reflecting in the strength distribution and thus the strength values were calculated for every specimen as a standard procedure.

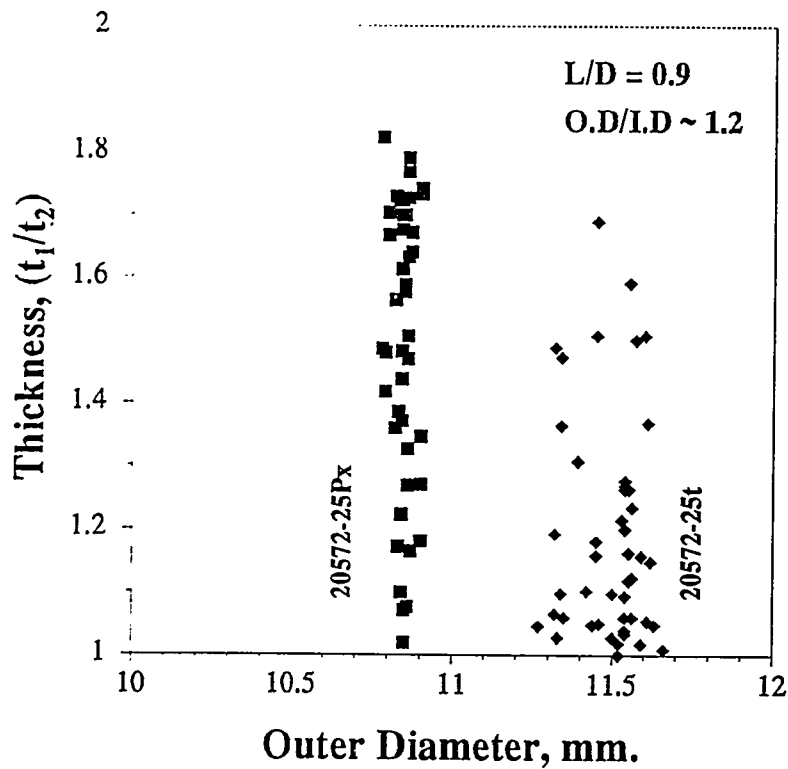


Fig 2. Variation in the C- ring specimen dimensions

### Strength of 20576 tubes:

The maximum fracture strength of the C-Ring specimens were calculated from the equation:

$$\sigma_{\theta_{\max}} = \frac{PR}{btr_o} \left[ \frac{r_o - r_a}{r_a - R} \right]$$

Where  $r_o$  - is the outer radius of the C-Ring,  $b$  - the width of the ring,  $t$  - thickness and  $P$  the fracture load. However, the actual fracture strength is calculated from the measure angle of fracture from the mid plane.

The measured strength of the 20576 tubes are as shown in table 1. The maximum strength of 429 MPa observed in 20576-25t was twice of that observed in 20576-25Px (210 MPa). However, the standard deviation in the strength values of 20576-25t was also higher than that observed in 20576-25Px. This could possibly be attributed to the variation observed in the specimen geometry.

Table1: Strength of 20576 tubes.

	20576-25 Px	20576- 25 t
Minimum, MPa	114.47	175.53
Maximum, MPa	210.43	429.18
Sum	1839.5628	3693.52
Points	11	12
Mean, MPa	167.23	307.79
Median, MPa	188.47	302.05
RMS, MPa	170.64	318.85
Std Deviation	35.62	86.95
Variance	1269.19	7561.61

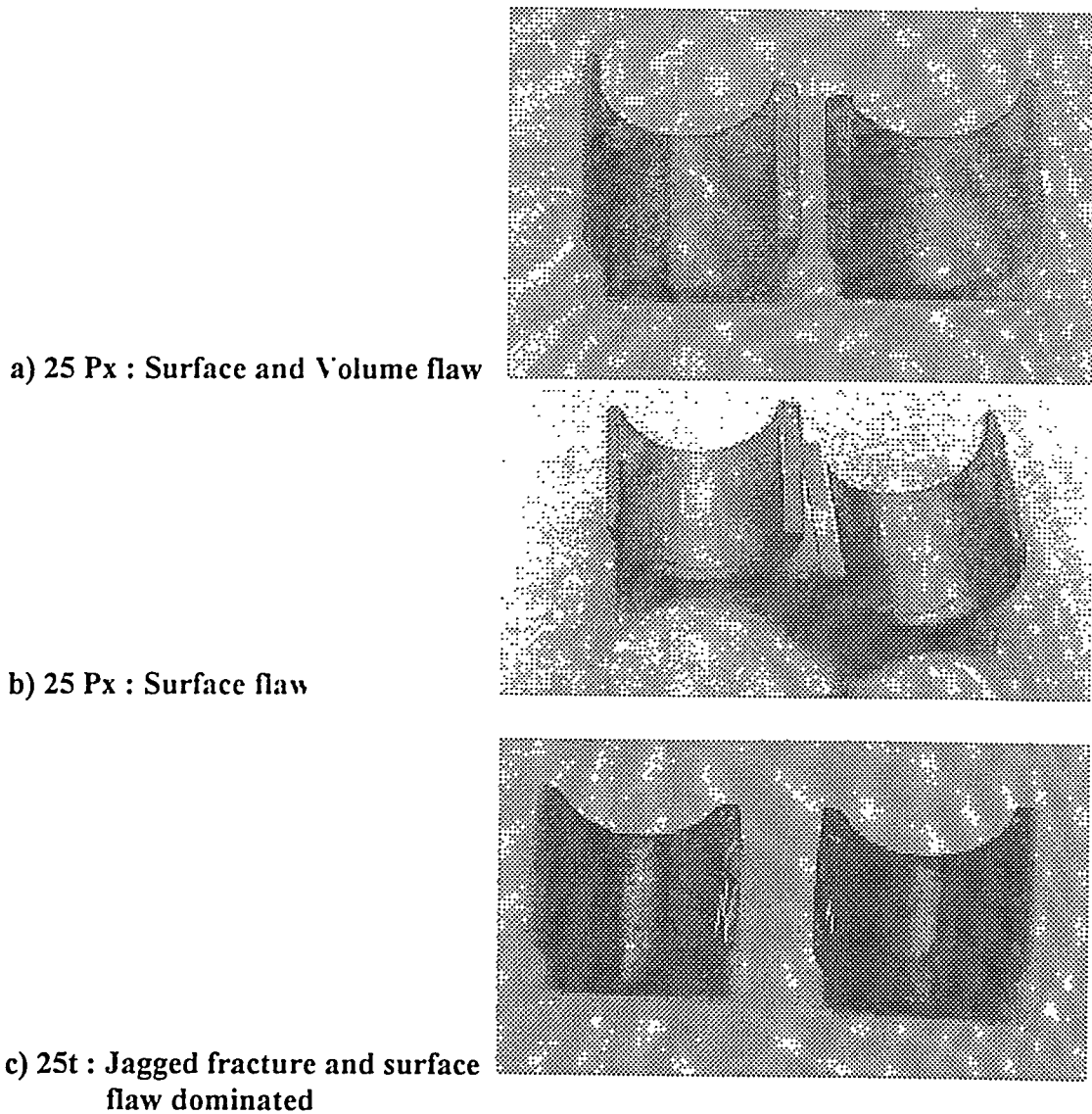
### Fracture Observations:

#### Macroscopic:

Macroscopic observation indicated a distinctive difference in fracture morphology of 20576-25Px and 20576-25t. In 25 Px, fractures in all the specimens tested were fractured at midplane. The fracture surfaces were smooth and seemingly dominated by surface flaws. On the other hand, specimens of 25t shattered during testing and very often the fracture plane was at an angle from the midplane. The fracture morphology was predominantly jagged with interspersing planes of smooth fracture.

Based on the macroscopic fracture observation, a simple two-parameter Weibull plot was generated to characterize the strength and the observed variation in wall thickness of individual

C-rings. A complete Weibull plot is to be generated from microscopic observation of fracture and the observed angle of fracture.



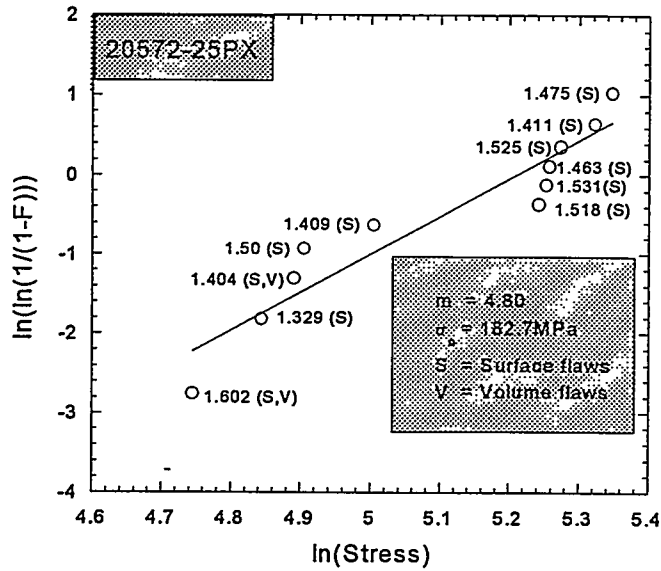
a) 25 Px : Surface and Volume flaw

b) 25 Px : Surface flaw

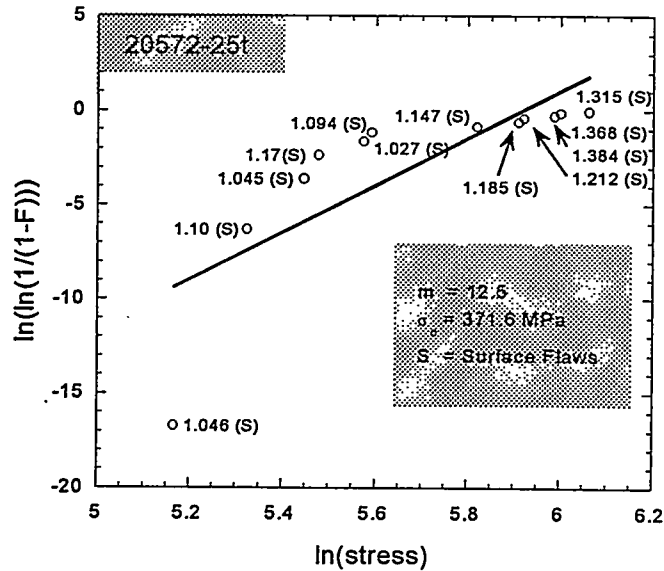
c) 25t : Jagged fracture and surface  
flaw dominated

Fig 3 Macroscopic fracture observed in 20576 tubes. a & b – Fracture dominated by surface and volume flaws in 25Px. The fracture is smooth and planar. c) Fracture in 25t is jagged and dominated by surface flaws.

A detailed fractographic study is planned to characterize the active fracture mechanism and the influence of preexisting flaws on the strength and fracture characteristics.



a) 20576-25Px



b) 20576-25t

Fig.4 Weibull plot of unadjusted strength distributions for all specimens tested at room temperature. The sample dimensions ( $t_1/t_2$ ) and observed macroscopic fracture are overlaid on the plot.

The Weibull plot indicated an increased Weibull modulus ( $m$ ) in the 25t samples as compared to 25Px specimens. The characteristic fracture stress  $\sigma_0$ , was also higher in 25t samples at 372 MPa as compared to 183 MPa for 25 Px samples.

# Task 4: Preparation and characterization of Dense Ceramic Oxygen Permeable Membrane

Dr. Harlan U. Anderson, Director of EMARC

Dr. Wayne Huebner, Dr. Yixiang Xie

University of Missouri- Rolla

## Summary

In this quarter, a modified Pechini liquid mixing method [1, 2] was used to produce mixed-cationic oxide powders of compositions,  $\text{La}_{0.19}\text{Sr}_{0.80}\text{Fe}_{0.90}\text{Cr}_{0.10}\text{O}_{3-\delta}$ ,  $\text{La}_{0.19}\text{Sr}_{0.80}\text{Fe}_{0.80}\text{Cr}_{0.20}\text{O}_{3-\delta}$ ,  $\text{La}_{0.19}\text{Sr}_{0.80}\text{Fe}_{0.65}\text{Cr}_{0.35}\text{O}_{3-\delta}$ ,  $\text{La}_{0.59}\text{Sr}_{0.40}\text{Fe}_{0.85}\text{Ti}_{0.15}\text{O}_{3-\delta}$ ,  $\text{La}_{0.59}\text{Sr}_{0.40}\text{Fe}_{0.85}\text{Cr}_{0.15}\text{O}_{3-\delta}$ ,  $(\text{La}_{0.60}\text{Sr}_{0.40})_{0.99}\text{FeO}_{3-\delta}$ ,  $\text{La}_{0.19}\text{Sr}_{0.80}\text{Fe}_{0.70}\text{Cr}_{0.20}\text{Ti}_{0.10}\text{Mg}_{0.01}\text{O}_{3-\delta}$ ,  $\text{La}_{0.19}\text{Sr}_{0.80}\text{Fe}_{0.70}\text{Cr}_{0.20}\text{Nb}_{0.10}\text{Mg}_{0.01}\text{O}_{3-\delta}$ ,  $\text{La}_{0.20}\text{Sr}_{0.80}\text{Fe}_{0.70}\text{Cr}_{0.20}\text{Ti}_{0.10}\text{O}_{3-\delta}$ , and  $\text{La}_{0.20}\text{Sr}_{0.80}\text{Fe}_{0.70}\text{Cr}_{0.20}\text{Nb}_{0.10}\text{O}_{3-\delta}$ , for phase study. Sintering process and x-ray diffraction study indicate 1) Cr doping should be restricted to a certain level, 2) a thermodynamic reversible process is recommended to avoid phase separation (decomposition), 3. A higher Sr doping should also combine with a Cr doping, 4)  $(\text{La}_{0.60}\text{Sr}_{0.40})_{0.99}\text{FeO}_{3-\delta}$  single phase can be reached by a reversible sintering process. After applying a stress on disk, XRD shows an orientation change. Sintered disks were sent to the MIT mechanical and sealing research group on their request.

## Introduction

Dense ceramic membrane materials have been studied by a team with NIST through Praxair and British Petroleum Chemical for use as oxygen separation membranes for gas production and syngas application. Leading dense ceramic membrane materials for high temperature oxygen separation have been identified, which are oxide perovskites with a general formula  $\text{ABO}_3$  with La, Sr at the A site and the B site primarily occupied by Fe. Due to the significant progress of the NIST program, a new team has been formed for further investigation on these materials through this UAF/DOE program.

As a part of the team, this group agreed to study the processes of making compositions, pressing, and sintering and to provide sintered disks using powders with selected compositions from  $\text{La}_x\text{Sr}_{1-x}\text{FeO}_{3-\delta}$  which is doped with either Ti, Cr, Ga, or Zr to other team members. Meanwhile this group engaged in characterization of the selected compositions through XRD, electrical conductivity, thermoelectric power measurements, TGA, and thermal expansion as the first phase task of the program. In our previous quarterly, semiannual, and annual reports through our XRD, TGA and thermal expansion study we have concluded that these oxides keep their major perovskite structure and are reversible at a temperature lower than 1000 °C in a strong reducing atmosphere up to 90% CO with a balance gas,  $\text{CO}_2$  ( $\log\text{PO}_2$ , -16.1). However, they lose phase stability in stronger reducing atmospheres, which is further confirmed by TGA and thermal expansion data. We also concluded that 1) instability of perovskite by A site Sr doping can be compensated by Fe multi-valence states. 2) B site Ti and Cr doping enhance the stability. Our previous research on non-ferrite lanthanum-strontium perovskite with Zr dopant indicates that Zr does not help phase stability possibly due to its larger radius than that of major B site element. We do not recommend Zr as a B site dopant. While these perovskites are not be able to maintain

a single phase under the wide application conditions, a composition of XRD single phase perovskite prepared under air atmosphere is absolutely necessary to establish a basis for a further intense study. Therefore, in this quarter, we have focused on the single phase composition study. Previous study on the high Sr doping composition,  $\text{La}_{0.19}\text{Sr}_{0.80}\text{FeO}_{3-\delta}$ , indicates that strontium oxide, SrO second phase is easy to be formed in the major perovskite matrix and reversibility is unlikely. To increase the perovskite single phase stability, either lower the Sr doping at A site or dope Cr at B site at an appropriate level.

## Experimental

### 1. Powder Preparation

A modified Pechini liquid mixing method [1, 2] was used to produce powders.

#### a) Chemicals

Vendor	Catalog No.	Name	Purity
Alfa Aesar	36665	Citric Acid, Monohydrate	99.0-102.0%
Fisher Scientific	E178-4	Ethylene Glycol	$\text{H}_2\text{O} < 0.02\%$
Fisher Scientific	A509SK-212	Nitric Acid	total metals $< 0.1\text{ppm}$
Alfa Aesar	16639	Lanthanum Carbonate	99.9%
Alfa Aesar	14343	Strontium Carbonate	99%
Alfa Aesar	33315	Iron (III) Nitrate	98.0-101.0%
		Niobium Oxalate	
Aldrich	32,525-2	Titanium diisopropoxide bis(acetyl-acetate)	
Alfa Aesar	11565	Chromium (III) Nitrate	98.5%

All metal compounds were quantified every two weeks and kept in tape sealed containers. For preparation of per 30 gram powder, the water, Citric Acid, and Ethylene Glycol content was 200 ml, 50 grams, and 20 grams respectively.

#### b) Processing

- (1) Citric Acid Monohydrate, and Ethylene Glycol are added into distilled water with magnetic stirring in a beaker.
- (2) Carbonate(s) is(are) added into the solution.
- (3) Slowly nitric acid was added into the liquid mixture until the liquid became transparent.
- (4) Dissolve nitrate(s) into the transparent liquid.
- (5) Filter the transparent liquid to eliminate dark solid insoluble residue.
- (6) Stir the liquid overnight.
- (7) Carefully evaporate water from the liquid on a hot plate until it solidifies.
- (8) Put the beaker into an oven at a temperature at about 150 EC for 48 hours.